

# Navigation of Concentric Tube Continuum Robots using Optimal Control

Siva Prasad Chakri Dhanakoti<sup>1</sup><sup>a</sup>, John H. Maddocks<sup>2</sup><sup>b</sup> and Martin Weiser<sup>3</sup><sup>c</sup>

<sup>1</sup>Department of Mathematics and Computer Science, Freie Universität Berlin, Berlin, Germany

<sup>2</sup>Institute of Mathematics, École Polytechnique Fédérale de Lausanne, Lausanne, Switzerland

<sup>3</sup>Zuse Institute Berlin, Berlin, Germany


**Keywords:** Optimal Control, Navigation, Path Planning, Gradient-based Optimization, Concentric Tube Continuum Robots.


**Abstract:** Recently developed Concentric Tube Continuum Robots (CTCRs) are widely exploited in, for example in minimally invasive surgeries which involve navigating inside narrow body cavities close to sensitive regions. These CTCRs can be controlled by extending and rotating the tubes one inside the other in order to reach a target point or perform some task. The robot must deviate as little as possible from this narrow space and avoid damaging neighbouring tissue. We consider *open-loop* optimal control of CTCRs parameterized over pseudo-time, primarily aiming at minimizing the robot's working volume during its motion. External loads acting on the system like tip loads or contact with tissues are not considered here. We also discussed the inclusion of tip's orientation in the optimal framework to perform some tasks. We recall a quaternion-based formulation of the robot configuration, discuss discretization, develop optimization objectives addressing different criteria, and investigate their impact on robot path planning for several numerical examples. This optimal control framework can be applied to any backbone based continuum robot.


## 1 INTRODUCTION

Concentric Tube Continuum Robots (CTCRs), also referred to as active cannulas, consist of concentric hollow elastic tubes of different stiffness and pre-curved. These tubes are usually made of shape memory alloy such as Nitinol which can undergo large elastic deformations, while avoiding plastic deformations. The concentric tubes of this robot are constrained to take the shape of a common centerline referred to as the backbone. This backbone is a smooth curve in the space, that can be controlled by sliding and rotating the tubes one inside the other. The tip of the robot is equipped with an instrument and is maneuvered by appropriate relative slides and twists of the tubes at its root. The slim shape of CTCRs motivated many researchers to utilize these devices in confined spaces, such as in minimally invasive surgeries (Burgner et al., 2011; Burgner et al., 2013; Al-falahi et al., 2020). The kinematic model describing the equilibria of these CTCRs is presented by (Rucker et al., 2010) using the *Cosserat rod* model.

Medical applications require suitable path planning and control strategies for performing the tasks with high precision. In surgical operations, damaging tissue along the robot length by lateral motions that stretch or sever neighboring tissue should be avoided. Therefore, paths with a minimum working space, i.e., a minimum deviation from a mean curve, are highly desirable. A *follow-the-leader* (FTL) strategy, where the robot is deployed telescopically such that the backbone always lies along the path traced by prior tip locations, occupies a minimal working space during its deployment and is an ideal solution for this purpose. The design and control parameters for achieving this deployment strategy are given by (Gilbert et al., 2015; Garriga-Casanovas and y Baena, 2018). In the simpler setup for this deployment, the unstressed tubes of the robot section must be either in the shape of circular arcs or in the shape of helical arcs with equal torsions. The robot backbone then assumes shape of a uniform curve like circular or helical arc under certain sets of control parameters. The sections are then extended along the curve's tangent such that the body traces its tip locus. This deployment fails when the constituent tubes are of unequal torsions or when the robot tip is mounted to a non-

<sup>a</sup> <https://orcid.org/0000-0001-8346-4289>

<sup>b</sup> <https://orcid.org/0000-0003-1127-8481>

<sup>c</sup> <https://orcid.org/0000-0002-1071-0044>

zero load. The working region must lie along this helical curve, so that this FTL deployment can reach the region, which is not the case in general. Some tasks like cardiac ablation (Yip et al., 2017) require the tip to move continuously to neighbouring points, necessarily deviating from the FTL configuration. Working just with FTL configurations limits the working space and degrees of freedom of the robot.

Suitable control techniques are necessary to control these robots so that they complete the required tasks in a minimal workspace or by deviating least from the FTL configuration. The necessary flexibility is usually given if the number of controls, i.e., lengths and twists of the tubes, exceeds the number of constraints on the tip position. For example, the robot tip can reach a point within reach for a wide range of control parameters. Appropriate control parameters should be chosen based on the complete motion path of the robot. The purpose of the current work is to investigate the impact of minimal working space path planning by formulating it as an optimal control problem. We also include the tip's orientation in the optimization framework to perform some tasks.

The kinematics of the robot is described through a set of ordinary differential equations (ODEs) in terms of its arclength (Rucker et al., 2010). A special set of control parameters lead to planar or uniform configurations that can be represented as simple helical curves (Gilbert et al., 2015). For the remaining cases, a boundary value problem (BVP) must be solved in order to obtain its state. We adopt a partially reduced approach by describing the robot states in terms of pseudo-time dependent control parameters, leading to a path planning problem in these parameters.

The use of optimal control techniques in CTCRs has been used for choosing design parameters based on the available workspace and anatomical constraints (Bergeles et al., 2015). Derivative-free optimization methods such as Nelder-Mead (Baykal et al., 2015; Granna et al., 2016) or particle swarm methods are used extensively. Gradient based optimization techniques are used only for simpler models (Lyons et al., 2009; Flaßkamp et al., 2019) where analytical derivatives are available. These methods lead to local minima rather than to global minima. But, they are computationally fast and useful in real-time operations. Tasks such as moving to a nearby point can usually be planned with local optimization methods. Recently, the use of nonlinear programming methods for CTRC path planning has been proposed by (Flaßkamp et al., 2019) in planar robots where analytical representation of the robot states is available. Here, we combine a collocation discretization of a quaternion-based kinematic description of CTCRs

with a collocation discretization of the equilibrium equations (BVPs) and a nonlinear programming approach, such that non-planar robots are also covered.

The paper is organized as follows. In Section 2, the kinematics of the CTCRs is briefly recalled and formulated in a quaternion setting. Then the system constraints and different objective functions are discussed in Sections 3 and 4. Discretization methods for translating the optimal control problem into a *nonlinear programming* (NLP) problem are discussed in Section 5. Finally, numerical examples making use of the proposed framework are presented in Section 6.

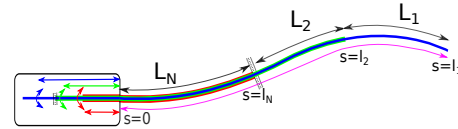


Figure 1: Schematic of the CTCR showing the notations and controls.

## 2 MECHANICAL MODEL

The continuum robots addressed in this paper are assumed to operate sufficiently slow, that the inertial effects are negligible. Therefore, the actual speed with which the task performed is irrelevant and a quasi-static model is used for the work. We assume perfectly elastic tubes, neglecting any possible hysteresis in the stress-strain relations. We also assume that no external forces act on the robot along its length or tip. A  $N$ -tubed CTCR consists of  $N$  concentric tubes of lengths  $l_1 \geq \dots \geq l_N$ , with the innermost tube being the longest. The different lengths  $l_k$  partition any configuration into  $N$  segments  $S_k$  each of length  $L_k := l_k - l_{k+1} \geq 0$  with the property each  $S_k$  consisting of  $k$  overlapping concentric tubes. The different lengths  $l_k$  partition the total length into  $N$  segments  $S_k$  of length  $L_k = l_k - l_{k+1} \geq 0$  such that  $S_k$  consists of  $k$  concentric tubes for  $k = 1, \dots, N$  as shown in Figure 1. For computational simplicity, the tubes for  $s < 0$  are considered with the angular feeds at  $s = 0$  and therefore, corresponds to the actual actuator feeds given by the operator. The section  $S_N$  is located at the proximal end and  $S_1$  is present at the distal end. The innermost tube of length  $l_1$  with *material frame* in its reference state is considered as backbone reference for our formulation and computations. The relative rotation of the constituent tubes about the common tangent is measured with respect to this reference. The configuration of the CTCR backbone (i.e., the innermost tube) is described as an orientable curve in 3D space described as a function of the arclength  $s \in [0, l_1]$  using a centerline  $\mathbf{r} : [0, l_1] \rightarrow \mathbb{R}^3$  and an attached or-

thonormal director frame

$$\mathbf{R}(s) = [\mathbf{d}_1(s), \mathbf{d}_2(s), \mathbf{d}_3(s)] \in \text{SO}(3), \quad (1)$$

where the axes of the *moving frame* called directors  $\mathbf{d}_i(s) \in \mathbb{R}^3$  are the columns of  $\mathbf{R}(s)$ . We derive the equilibria explicitly in terms of position vector  $\mathbf{r}(s)$  and quaternions  $\mathbf{q}(s)$  as a system of ODEs in a similar manner of Hamiltonian Formulation of rods (Dichmann et al., 1996). Quaternions or Euler parameters  $\mathbf{q}(s) \equiv (q_1, q_2, q_3, q_4) : [0, l_1] \rightarrow \mathbb{S}^4$  of unit length, i.e.,  $|\mathbf{q}(s)| = 1$  are used in this model. They characterize the director frame  $\mathbf{R}(s)$  by

$$\mathbf{d}_1(s) = \begin{bmatrix} q_1^2 - q_2^2 - q_3^2 + q_4^2 \\ 2(q_1q_2 + q_3q_4) \\ 2(q_1q_3 - q_2q_4) \end{bmatrix}, \quad (2a)$$

$$\mathbf{d}_2(s) = \begin{bmatrix} 2(q_1q_2 - q_3q_4) \\ -q_1^2 + q_2^2 - q_3^2 + q_4^2 \\ 2(q_2q_3 + q_1q_4) \end{bmatrix}, \quad (2b)$$

$$\mathbf{d}_3(s) = \begin{bmatrix} 2(q_1q_3 + q_2q_4) \\ 2(q_2q_3 - q_1q_4) \\ -q_1^2 - q_2^2 + q_3^2 + q_4^2 \end{bmatrix}. \quad (2c)$$

For brevity, the dependence of  $q_i$ ,  $i = 1, \dots, 4$  on  $s$  is omitted. The director  $\mathbf{d}_3$ -axis is aligned along the tangent of the curve centreline for inextensible and unsharable rods. The spatial evolution of the frame with respect to the arclength  $s$  is described with the help of the Darboux vector  $\mathbf{u} : [0, l_1] \rightarrow \mathbb{R}^3$  through the relations  $\mathbf{d}_i'(s) = \mathbf{u}(s) \times \mathbf{d}_i(s)$ ,  $i = 1, 2, 3$ , where  $\times$  denotes the cross-product in  $\mathbb{R}^3$ . The strain components  $\mathbf{u}(s) \cdot \mathbf{d}_j(s) \equiv u_j(s)$  are obtained from the quaternions  $\mathbf{q}(s)$  through the relation

$$u_j(s) = 2\mathbf{B}_j\mathbf{q}(s) \cdot \mathbf{q}'(s), \quad j = 1, 2, 3, \quad (3)$$

where  $\mathbf{B}_i$  are  $4 \times 4$  skew symmetric matrices given by

$$\mathbf{B}_1 = \begin{bmatrix} 0 & 0 & 0 & 1 \\ 0 & 0 & 1 & 0 \\ 0 & -1 & 0 & 0 \\ -1 & 0 & 0 & 0 \end{bmatrix}, \mathbf{B}_2 = \begin{bmatrix} 0 & 0 & -1 & 0 \\ 0 & 0 & 0 & 1 \\ 1 & 0 & 0 & 0 \\ 0 & -1 & 0 & 0 \end{bmatrix},$$

$$\mathbf{B}_3 = \begin{bmatrix} 0 & 1 & 0 & 0 \\ -1 & 0 & 0 & 0 \\ 0 & 0 & 0 & 1 \\ 0 & 0 & -1 & 0 \end{bmatrix}$$

These matrices, acting on  $\mathbf{q} \in \mathbb{R}^4$ , result in orthogonal vectors for  $\mathbf{i} \neq \mathbf{j}$  (i.e.,  $\mathbf{B}_i\mathbf{q} \cdot \mathbf{B}_j\mathbf{q} = 0$ ) and give the quaternion length when  $\mathbf{i} = \mathbf{j}$  as  $\mathbf{B}_i\mathbf{q} \cdot \mathbf{B}_i\mathbf{q} = \|\mathbf{q}\|^2 = 1$ . The tubes are considered to be uniform, inextensible, unsharable and transversely constitutively isotropic with stiffness matrix  $\mathbf{K}^{[i]} = \text{diag}(K_{11}^{[i]}, K_{11}^{[i]}, K_{33}^{[i]})$  and precurvatures  $\hat{\mathbf{u}}^{[i]} = [\hat{u}_1^{[i]}, \hat{u}_2^{[i]}, \hat{u}_3^{[i]}]^T$ . Each concentric

tube has a constant stiffness matrix  $\mathbf{K}^{[i]}$  along its length. As a notational convenience, we use a specific step function  $\mathbf{K}^{[k]}(s)$  to extend it to a zero function beyond its length  $l_k$  as

$$\mathbf{K}^{[k]}(s) = \begin{cases} \mathbf{K}^{[k]}, & s \in [0, l_k], \\ 0, & s \in (l_k, l_1]. \end{cases} \quad (4)$$

Here,  $l_k$  is the length of the  $k$ -th tube calculated from  $s = 0$  and is related to the lengths of the overlapping regions  $L_i$  as  $l_k = \sum_{i=k}^N L_i$ . Let  $\alpha^{[i]} : [0, l_i] \rightarrow \mathbb{R}$ ,  $i = 2, \dots, N$  be the relative angle of twist between the tube  $i$  and the reference innermost tube (tube 1) and

$$\mathbf{R}_z(\alpha) := \begin{bmatrix} \cos \alpha & -\sin \alpha & 0 \\ \sin \alpha & \cos \alpha & 0 \\ 0 & 0 & 1 \end{bmatrix}$$

be the rotation matrix about the variable tangent  $\mathbf{d}_3$ -axis. The minimization of the total strain energy (Rucker et al., 2010) of the system of concentric tubes yields the shape  $\tilde{\mathbf{u}} \in \mathbb{R}^3$  and effective stiffness  $\mathbf{K}_{\text{eff}}$  of the CTCR backbone as

$$\tilde{\mathbf{u}}(s) = \mathbf{K}_{\text{eff}}^{-1}(s) \sum_{i=1}^N \mathbf{K}^{[i]}(s) \mathbf{R}_z(\alpha^{[i]}(s))^T \check{\mathbf{u}}^{[i]}, \quad (5)$$

$$\mathbf{K}_{\text{eff}}(s) = \sum_{i=1}^N \mathbf{K}^{[i]}(s),$$

with  $\check{\mathbf{u}}^{[i]} = [\hat{u}_1^{[i]}, \hat{u}_2^{[i]}, \hat{u}_3^{[i]} - \alpha^{[i]'}(s)]^T$ . Finally, the equilibrium configuration of the robot in terms of its position vector  $\mathbf{r}(s)$ , quaternions  $\mathbf{q}(s)$  and the relative twist angle  $\alpha^{[i]}(s)$  is given by the following set of first order ODEs

$$\mathbf{r}'(s) = \mathbf{d}_3(s), \quad \text{in } ]0, l_1[,$$

$$\mathbf{q}'(s) = \sum_{j=1}^3 \tilde{u}_j(s) \frac{1}{2} \mathbf{B}_j \mathbf{q}(s), \quad \text{in } ]0, l_1[,$$

$$\alpha^{[i]'}(s) = \frac{\sum_{j=2}^i \beta^{[j]}(s)}{K_{33}^{[1]}(s)} + \frac{\beta^{[i]}(s)}{K_{33}^{[i]}(s)} + \hat{u}_3^{[i]}(s) - \hat{u}_3^{[1]}(s), \quad \text{in } ]0, l_i[, \quad (6)$$

$$\beta^{[i]'}(s) = \frac{K_{11}^{[i]}(s) \hat{u}_1^{[i]}(s)}{\sum_{j=2}^i K_{11}^{[j]}(s)}$$

$$\left( \sum_{j=1}^i K_{11}^{[j]}(s) \hat{u}_1^{[j]} \sin(\alpha^{[i]}(s) - \alpha^{[j]}(s)) \right), \quad \text{in } ]0, l_i[,$$

for the  $i = 2, \dots, N$  outer tubes. The term  $\alpha^{[1]}(s) = 0$  by definition. The last two terms are the result of Euler-Lagrange equations on the total elastic strain

energy of the system and  $\beta^{[i]}$  is the canonical momentum conjugate to  $\alpha^{[i]}$  and it gives the twist moment in the  $i$  th tube. The boundary conditions are specified in terms of alignment of the innermost tube frame and relative rotation of the other tubes at the root as

$$\begin{aligned} \mathbf{r}(0) = 0, \quad \mathbf{q}(0) &= [0, 0, \sin \theta_1, \cos \theta_1], \\ \alpha^{[i]}(0) &= \alpha_o^{[i]}, \quad \beta^{[i]}(l_i) = 0, \quad i = 2, 3, \dots, N, \end{aligned} \quad (7)$$

where the conditions on  $\beta^{[i]}$  corresponds to *natural boundary conditions*. The tube  $k$  is not present for  $s > l_k$  and hence it has no contribution for the deformation of the backbone for  $s \in [l_k, l_1]$ . The  $\mathbf{d}_1 - \mathbf{d}_2$  plane of the reference tube (inner tube) at the root ( $s = 0$ ) coincides with the fixed laboratory  $\mathbf{e}_1 - \mathbf{e}_2$  plane. The angle  $\theta_1$  corresponds to the angle of rotation of the reference frame of inner tube about  $\mathbf{e}_3 \equiv \mathbf{d}_3$ -axis at  $s = 0$  and is controlled by the user. The shape  $(\mathbf{r}, \mathbf{q})$  must be continuous across the boundary between the sections without any kinks. The robot is controlled by varying the lengths  $L_i$  of the segments, i.e., the feed of the tubes, and by varying the initial conditions on  $\alpha_o^{[i]}$ , i.e., the rotation of the tubes at the root. Note that any discretization needs to take the coefficient discontinuities at the segment boundaries  $l_i$  into account for achieving the nominal approximation order, e.g. by positioning grid points at the segment boundaries or by formulating the boundary value problem as a sequence of smaller boundary value problems coupled by appropriate boundary conditions. The latter approach is followed here.

By solving the boundary value problem (6)–(7), the equilibrium configuration of the robot i.e., its  $\mathbf{r}(\mathbf{y}; s)$  and  $\mathbf{q}(\mathbf{y}; s)$  are obtained as a function of control parameter vector  $\mathbf{y}$  which is defined as

$$\mathbf{y} := [L_1, \dots, L_N, \theta_1, \dots, \theta_N] \in \mathbb{R}^{2N}.$$

Here,  $\theta_i = \theta_1 + \alpha_o^{[i]}$ ,  $i = 2, \dots, N$  is the angle of rotation of the  $i$ -th tube. Thus, a CTCR with  $N$  tubes has  $2N$  controls parameters determining its spatial configuration.

### 3 SYSTEM KINEMATICS

In the path planning task, the motion of the robot is parameterized over pseudo-time  $t \in T := [0, 1]$ , since the actual speed of the motion is not relevant in a quasi-static model. The control parameters  $\mathbf{y}$  at time  $t$  are written as  $\mathbf{y}(t)$ . A control rate vector  $\mathbf{v}(t) = [u_1(t), \dots, u_N(t), \gamma_1(t), \dots, \gamma_N(t)]$  and an initial

value  $\mathbf{y}_0$  are introduced to describe the system dynamics defined as

$$\dot{\mathbf{y}}(t) = \mathbf{v}(t), \quad \mathbf{y}(0) = \mathbf{y}_0. \quad (8)$$

The rates  $v_i : T \rightarrow \mathbb{R}$  and  $\gamma_i : T \rightarrow \mathbb{R}$  model the traverse and rotational velocities of each tube, respectively. The system dynamics (8) ensures the continuity of control parameters on the whole time interval  $T$ . The control parameters corresponding to the rotation of the tubes, i.e.,  $\theta_i$ ,  $i = 1, \dots, N$  can take any real value (being  $2\pi$ -periodic), whereas the feed parameters  $L_i$ ,  $i = 1, \dots, N$  can take only non-negative values and are bounded by the maximum length of the tubes  $L_{i,\max}$  resulting in the inequality constraint,

$$0 \leq L_i(t) \leq L_{i,\max} \quad \forall t \quad i = 1, \dots, N. \quad (9)$$

Elastic instabilities like *snapping* can occur in these CTCRs resulting in the sudden release of elastic strain energy (Gilbert et al., 2016). Such situations are avoided by using tubes shorter than a critical length  $L_{crit}$ .

## 4 OBJECTIVE FUNCTIONS

The task of navigating a robot in the best way is quantified in terms of some objective function to be minimized. Here, we consider prototypical objective functions describing simple tasks.

**Target Position:** The primary goal for most robot tasks is to maneuver the robot such that its tip reaches a target point  $\mathbf{r}_{tar}$  and orientation  $\mathbf{q}_{tar}$  at the final time  $t = 1$ . Obtaining a configuration simultaneously satisfying the position and orientation requirements is not always possible, especially with a small number of tubes, say,  $N \leq 3$ . This requirement is best included in the objective as a final time penalty:

$$\begin{aligned} M_1(\mathbf{y}) := & \|\mathbf{r}(\mathbf{y}(1), l_1) - \mathbf{r}_{tar}\|^2 \\ & + \lambda \|\mathbf{q}(\mathbf{y}(1), l_1) - \mathbf{q}_{tar}\|^2, \end{aligned} \quad (10)$$

where  $\lambda$  is the weighing term useful for prioritizing between tip's position and orientation with  $\|\cdot\|$  the Euclidean norm. The robot state  $\mathbf{r}(\mathbf{y}(t); s, t)$ ,  $\mathbf{q}(\mathbf{y}(t); s, t)$  is obtained after solving the boundary value problem (6)–(7) with control parameters  $\mathbf{y}(t)$ . Alternatively, reaching the target position and orientation could be specified as equality constraints, but since many combinations of position and orientation are not exactly achievable, this would render the optimization task infeasible. Thus, relaxing this requirement in form of a deviation penalty in the objective is an attractive strategy. An alternative target requirement is to specify only the desired tangent

of the tip, i.e.,  $\mathbf{d}_3(\mathbf{y}(1), l_1)$ , instead of the whole orientation. In this case, the condition is imposed only on a single director instead of all three director axes, leaving the freedom of rotations around the robot tip tangent. As the directors are normalized, this can be formulated as minimizing the scalar product of the director and a given target direction:

$$M_1(\mathbf{y}) := \|\mathbf{r}(\mathbf{y}(1), l_1) - \mathbf{r}_{\text{tar}}\|^2 - \lambda \mathbf{d}_3(\mathbf{y}(1), l_1) \cdot \mathbf{r}_{\text{tar}} \quad (11)$$

**Path Tracing:** Some applications may require the tip to follow a prescribed curve  $\mathbf{r}_{\text{path}}(t)$  and orientation  $\mathbf{n}_{\text{path}}(t)$ . These problems are dealt by including a Lagrange term in the objective function as

$$J_1(\mathbf{y}) := \int_0^1 (\|\mathbf{r}(\mathbf{y}(t), t) - \mathbf{r}_{\text{path}}(t)\|^2 - \lambda \mathbf{d}_3(\mathbf{y}(t), l_1) \cdot \mathbf{n}_{\text{path}}(t)) dt \quad (12)$$

**Covered Volume:** Minimizing the working volume of the robot i.e., the space traversed by it when performing a task, is another quantity of interest. There are several ways in which the working volume could be quantified. One possible solution is the accumulated deviation from the reference *Follow the Leader* configuration  $\mathbf{r}(\mathbf{y}_{\text{FTL}}, s)$ . To perform or initiate any task, the robot tip has to reach an initial point through a FTL strategy with control parameters  $\mathbf{y}_{\text{FTL}}$  and move from this position to trace a desired path. We take the  $\mathbf{r}(\mathbf{y}_{\text{FTL}}, s)$  configuration as a reference and measure the robot's deviation from this configuration, which yields a rough measure of the working volume. The smaller the deviation from the reference is, the lower the robot's interference with the neighboring tissues. The corresponding objective is

$$J_2(\mathbf{y}) := \int_{t=0}^1 \int_{s=0}^{l_1(t)} d(\mathbf{r}(\mathbf{y}_{\text{FTL}}, s), \mathbf{r}(\mathbf{y}(t), s)) ds dt, \quad (13)$$

where  $d(\hat{\mathbf{r}}, \mathbf{r}(s))$  is the distance of  $\mathbf{r}(s)$  from the reference configuration  $\hat{\mathbf{r}}$ . This is defined as the distance to the arclength projection, i.e.,

$$d(\hat{\mathbf{r}}, \mathbf{r}(s)) = \|\hat{\mathbf{r}}(s') - \mathbf{r}(s)\| \quad \text{with} \quad \int_{\sigma=0}^{s'} \hat{\mathbf{r}}'(\sigma) d\sigma = s. \quad (14)$$

Note that in the FTL configuration the innermost tube can be assumed to have an infinite length, such that the FTL arclength always exceeds  $s$  and the projection (14) is well-defined. A closely related, but quantitatively different means to quantify the working volume of the robot is the area swept by the robot during its navigation, which is given by

$$J_2(\mathbf{y}) := \int_{t=0}^1 \int_{s=0}^{\Sigma L_i(t)} \mathbf{r}'(s, t) \times \frac{\partial}{\partial t} \mathbf{r}'(s, t) ds dt. \quad (15)$$

**Regularization:** In addition, the square of the  $L_2$ -norm of the  $\mathbf{v}(t)$  vector is included as a regularization term in the objective function to avoid high-frequency instabilities,

$$J_3(\mathbf{v}) := \int_{t=0}^1 \|\mathbf{v}(t)\|^2 dt.$$

Furthermore, the solution can also be subjected to path constraints of the form

$$\mathbf{g}_l \leq \mathbf{g}(\mathbf{Y}, t) \leq \mathbf{g}_u, \quad (16)$$

where  $\mathbf{g} \in \mathbb{R}^g$  is some objective function depending on the robot's state and control parameters. One possible example is maintaining bounds on the robot tip orientation in a task.

In total, we define the objective as a linear combination of the individual contributions discussed above,

$$J(\mathbf{y}, \mathbf{v}) = \lambda_0 M_1(\mathbf{y}) + \lambda_1 J_1(\mathbf{y}) + \lambda_2 J_2(\mathbf{y}) + \lambda_3 J_3(\mathbf{v}).$$

Depending on the application, some of the objective terms can be more important than others, and may be emphasized by a corresponding selection of the weights  $\lambda_i$ . Thus, we obtain the optimal control problem

$$\min_{\mathbf{y} \in H^1(T), \mathbf{v} \in L^2(T)} J(\mathbf{y}, \mathbf{v}) \quad (17)$$

subject to equality constraints (8) and inequality constraints (9) and (16).

## 5 DISCRETIZATION

Solving the optimal control problem numerically requires a combination of discretization and optimization methods. We follow the *discretize-then-optimize* approach, also known as the direct method, and discretize the optimal control problem (17) in pseudo-time  $t$  and arclength  $s$  in order to translate the problem into a *Non-linear Programming* (NLP) problem to be solved (Nocedal and Wright, 2006; Betts, 2010). We divide the time interval  $[0, 1]$  into  $m$  sub-intervals at time points  $0 = t_0 < t_1 \cdots < t_m = 1$ , in the simplest case with equidistant steps of length  $t_{i+1} - t_i = \frac{1}{m}$ . The objective function is then approximated on these time intervals using the trapezoidal rule as

$$J_m = \lambda_0 M_1 + \frac{1}{m} \left( \frac{1}{2} \bar{J}(0) + \sum_{i=1}^{m-1} \bar{J}(t_i) + \frac{1}{2} \bar{J}(1) \right),$$

where  $\bar{J}(t) = \lambda_1 J_1 + \lambda_2 J_2 + \lambda_3 J_3$ . The state  $\mathbf{r}(s), \mathbf{q}(s)$  of the robot is obtained for the controls  $\mathbf{y}(t_k)$  at the time points  $t_k$  by discretizing and solving the *bvp*

Table 1: Parameters of the CTCR used in the examples..

Option	Tube 1	Tube 2	Tube 3
Bending Stiffness $K_{11}^{[i]} (\times 10^4 N.mm^2)$	1.0	1.2	1.4
Torsion Stiffness $K_{33}^{[i]} (\times 10^4 N.mm^2)$	1.0/1.3	1.2/1.3	1.4/1.3
Precurvature vector ( $mm^{-1}$ )	[1/200,0,0]	[1/125,0,0]	[1/100,0,0]
Maximum Length ( $mm$ )	330	220	110

problem (6), (7) using suitable collocation methods (Kierzenka and Shampine, 2008) converting the infinite dimensional problem to an algebraic equation system. From the robot state, the objective functions  $j(t_k)$  are computed, where the integrals along the robot's length arising in (13) are approximated again using the trapezoidal rule. The ODEs (8) in the system dynamics are approximated using central differences as

$$\frac{\mathbf{y}_i(t_{k+1}) - \mathbf{y}_i(t_k)}{t_{k+1} - t_k} = \mathbf{v}_i(t_{k+1/2}) \quad (18)$$

for  $i = 0, \dots, m-1$  in terms of the pseudo-velocities  $\mathbf{v}_i(t_{k+1/2})$ . The direct discretization results in a nonlinear program with  $4Nm$  variables and  $2Nm$  equality constraints. This NLP problem can be solved numerically using a variety of available methods. Direct methods use gradient-based techniques for solving the NLP and they require the gradient information of the objective function and constraints. As some of the objective terms are functions of solutions of the *bvp*, analytical derivatives are not readily available. Instead, derivatives can be obtained by algorithmic differentiation or approximated by simple finite differences (Griewank and Walther, 2000). For simplicity of implementation, we use forward difference schemes. The gradients are computed using IVP finite difference scheme in a similar manner as that in (Rucker and Webster, 2011) and then supplied in the sub-routines.

## 6 NUMERICAL EXAMPLES

We demonstrate the proposed optimal control framework using a 3-tube CTCR. The mechanical properties of the constituent tubes are given in Table 1. We consider tasks like guiding the robot tip to a prescribed point and guiding it to a prescribed orientation. These numerical examples are solved with Matlab's *fmincon* which uses an interior point algorithm (Nocedal and Wright, 2006).

### 6.1 Minimum Working Volume

In the first example, we consider maneuvering the robot tip to a specified point  $\mathbf{r}_{\text{tar}}$ . Here, the orientation and the path of the tip  $\mathbf{r}_{\text{path}}(t)$  are not important and not accounted for in the overall objective i.e.,  $\lambda = 0$  in (10) and  $\lambda_1 = 0$ . The effectiveness of the proposed *minimum deviation objective* in reducing the working volume is examined by comparing the cases with  $\lambda_2 = 0, 50$  and 200. Fixed values of  $\lambda_0 = 400$  and  $\lambda_3 = 5$  are used throughout this subsection. The curve corresponding to the *follow-the-leader* configuration with controls  $\mathbf{y}_{\text{FTL}} = [0.5, 0.5 + \pi, 0.5 + \pi, 0.4, 0.6, 0.5]$  is used as reference or mean curve, and for calculating the objective (13). An initial configuration corresponding to the control parameters  $\mathbf{y}(0) = [0.5, 3.64, 3.84, 0.4, 0.6, 0.5]$  is used for all the examples and a target  $\mathbf{r}_{\text{tar}} = (-0.4, 0.0, 1.0)$  are chosen. No path constraints (16) are considered in this task. The solution consisting of states corresponding to the control parameters  $\mathbf{y}(0)$  is given as initial guess at all time steps  $t_k \in [0, 1]$ . The optimization is carried out using these parameters and states. The evolution of the robot configurations and its control parameters  $\mathbf{y}(t)$  in the time interval  $[0, 1]$  are shown in Figure 2.

When the coefficient of the *minimum deviation measure*  $J_2$ , i.e.  $\lambda_2$  is zero, the objective is to reach the target  $\mathbf{r}_{\text{tar}}$  with the minimum regularization energy. As a result, the control parameters are obtained as a linear function in the time interval  $[0, 1]$  as can be seen in Figure 2b. It appears qualitatively in Figure 2a that the robot occupies minimum working space during a maneuver task for higher values of  $\lambda_2$  and is supported by the corresponding values of the deviation measure shown in Table 2. When the penalty for the deviation term is non-zero, the robot navigated with a minimum deviation path by reducing its length in the period of its maneuver and extending its length in the final period. These optimal solutions continuously depend on the solution at initial time  $t = 0$ . The obtained optimal solutions depend on the initial guess and they vary if another initial guess is used.

The effect of using sweep area (15) as a minimum volume measure is examined by comparing its values

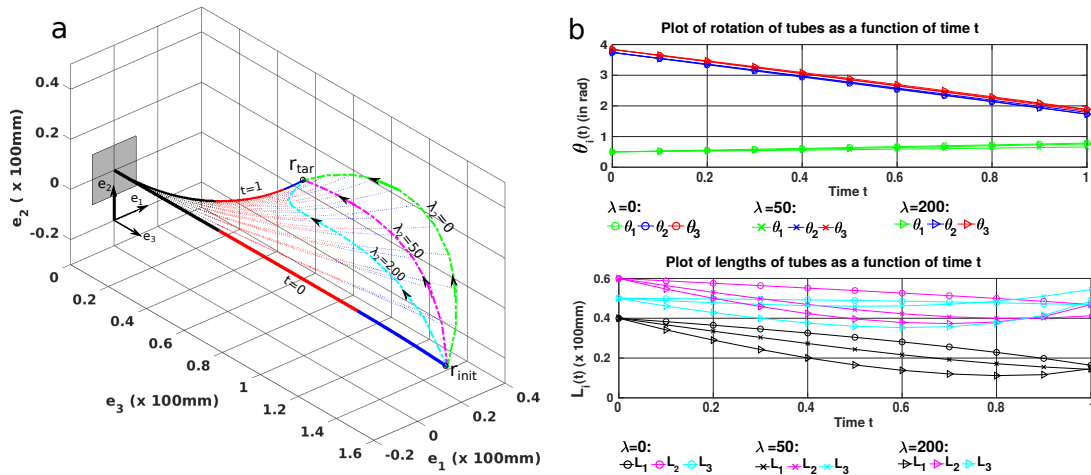


Figure 2: (a) 3D views of the robot evolution with its tip  $\mathbf{r}_{\text{tar}}$  from  $\mathbf{r}_{\text{init}}$  with different penalization of volume minimization objectives. The robot's sections are shown in different colours with black, red and blue corresponding to sections with 3, 2, and 1 tube, respectively. The trace of the tip is shown in green, magenta and cyan. The initial and final states of CTCR are shown in solid lines whereas the intermediate states are shown in dotted lines. (b) The evolution of control parameters  $\mathbf{y}(t)$  for different  $\lambda_2$ . The curves of rotation parameters  $\theta_i(t)$  for all cases of  $\lambda$  almost coincide. The markers correspond to the mesh used for the computations. The control parameters at  $t = 1$  for all three cases are different, but correspond to the same tip point.

Table 2: Effect of the penalizing term  $\lambda_2$  on the deviation term (as calculated in (13) and the objective.

$\lambda_2$	Deviation term value $J_2$	Objective $J$
0	0.0544	20.4121
50	0.0220	21.8843
100	0.0162	22.8030
200	0.0107	23.9423

for different penalizing terms in Table 3. Increase of the penalizing terms resulted in the decrease of the sweep area measure  $J_2$ , demonstrating the effectiveness of the optimization framework.

Table 3: Effect of the penalizing term  $\lambda_2$  on the sweep area and the objective..

$\lambda_2$	Sweep area $J_2$	Objective $J$
0	0.4586	20.4121
5	0.2716	22.9218
10	0.2117	24.0679
20	0.1712	25.2532

## 6.2 Maintaining Fixed Tip Orientation

In this example, we include the tip orientation as well as the target path  $\mathbf{r}_{\text{path}}(t)$  in the optimal problem. The goal is to maneuver the robot tip close to a prescribed path  $\mathbf{r}_{\text{path}}(t)$  with a restriction on the tip's orientation  $\mathbf{d}_3(\mathbf{y}(t), l_1)$ . The straight line between the initial point  $\mathbf{r}_{\text{init}}$  and the target  $\mathbf{r}_{\text{tar}}$  is specified as tar-

get path as  $\mathbf{r}_{\text{path}}(t) = (1-t)\mathbf{r}_{\text{init}} + t\mathbf{r}_{\text{tar}} \forall t \in [0, 1]$ . The tip's tangent of the initial state ( $t = 0$ ) is taken as  $\mathbf{n}_{\text{tar}}$  for this example. Therefore, the goal is to move to the target  $\mathbf{r}_{\text{tar}}$  with minimum deviation of its tip's tangent from  $\mathbf{n}_{\text{tar}}$ . The penalization of the tip orientation deviation is considered by using different values of  $\lambda$ . The *minimum deviation* objective  $J_2$  is not considered here: since the tip is constrained to move along a path  $\mathbf{r}_{\text{path}}(t)$ , its effect would be negligible.  $\lambda_0 = 5$ ,  $\lambda_1 = 400$ ,  $\lambda_2 = 0$ ,  $\lambda_3 = 5$  are used in this example. The time interval  $[0, 1]$  is discretized into 10 equal intervals and 10 points on the straight line are obtained. The evolution of robot and the angle between its tip tangent and the  $\mathbf{n}_{\text{tar}}$  for different values of  $\lambda$  are plotted in Figure 3. However, not all specified target points can be reached without violating the orientation constraints. For such points, the robot does not reach the specified point  $\mathbf{r}_{\text{tar}}$ . It gets to a position as closer to  $\mathbf{r}_{\text{tar}}$  while satisfying the orientation restriction.

## 6.3 Changing the Tip Orientation without Changing Its Position

In the final example, we consider a task where the robot tip is guided to a prescribed orientation  $\mathbf{n}_{\text{tar}}$  without changing its position. For this purpose, the prescribed path in (12) is specified as a single point, i.e.,  $\mathbf{r}_{\text{path}}(t) = \mathbf{r}_{\text{tar}}$ . The optimization is carried out by penalizing the deviation of the robot tip from the target  $\mathbf{r}_{\text{tar}}$ . The penalizing terms  $\lambda_0 = 400$ ,  $\lambda_1 = 100$ ,

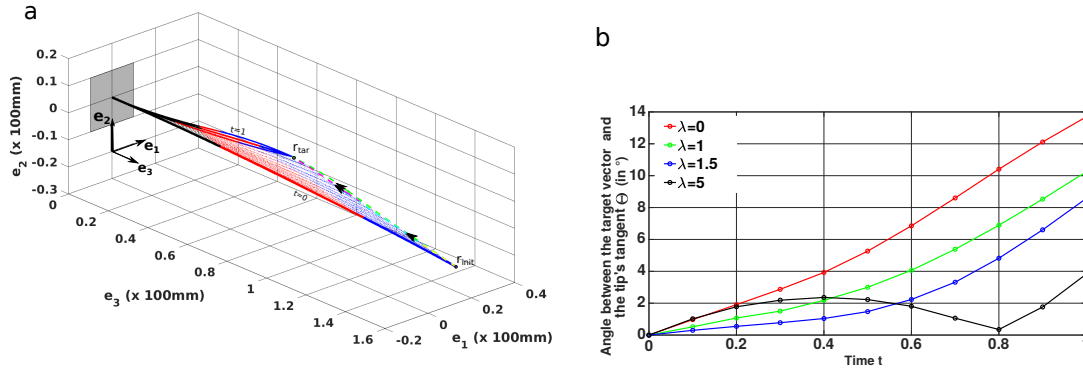


Figure 3: (a) The evolution of the CTCR as its tip moves from an initial point  $\mathbf{r}_{init}$  to a target  $\mathbf{r}_{tar} = [-0.01, 0.12, 0.78]$ . The tip is constrained to move along the straight line connecting  $\mathbf{r}_{init}$  and  $\mathbf{r}_{tar}$  by penalizing the deviation of the tip from the path. The robot tip is guided closely to the specified target vector  $\mathbf{n}_{tar}$  by using non-zero penalization terms  $\lambda$  in (12). The traces of the tip for different values of  $\lambda$  are shown. These traces are very close to each other. (b) The plots of the angle  $\Theta$  between the tip and the target vector  $\mathbf{n}_{tar}$  during the robot's navigation for different values of  $\lambda$ .

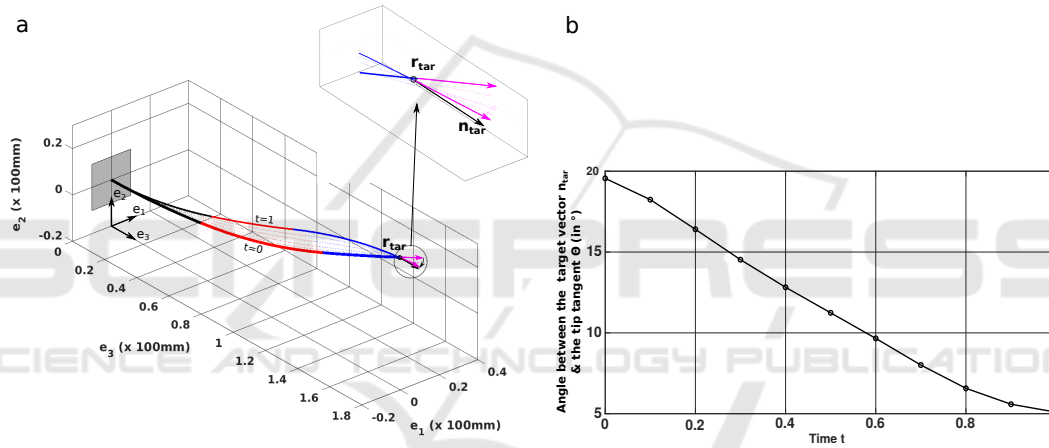


Figure 4: Example illustrating the maneuver of robot with its tip staying close to the initial tip point  $\mathbf{r}_{init} \equiv \mathbf{r}_{tar}$  and the tip tangent (in magenta) approaching the specified target  $\mathbf{n}_{tar} = [0, 0, 1]^T$  (in black). The enlarged view of the region around the tip is shown clearly indicating the tangents of the tip and the target  $\mathbf{n}_{tar}$ . The tip deviates slightly from the  $\mathbf{r}_{tar}$  during this process. There is a slight difference of  $5^\circ$  angle between the tip's tangent of the final state and the  $\mathbf{n}_{tar}$  at the final time ( $t = 1$ ).

$\lambda_2 = 0$  and  $\lambda_3 = 5$  are used for the implementation. The configurations of the robot as its tip changes its orientation to the target  $\mathbf{n}_{tar} = [0, 0, 1]^T$ , while its position staying close to the target  $\mathbf{r}_{tar}$ , are shown in Figure 4. The tip's orientation might not reach every specified target orientation as configurations with such orientation are not feasible. In such cases, the tip just gets closer to the  $\mathbf{n}_{tar}$  and does not reach it.

## 7 CONCLUSIONS

Our work has presented a mathematical model for guiding the robot in its workspace using optimal control techniques. The robot's navigation is modelled as a constrained optimal control problem and a suit-

able numerical strategy for its solution is described. The numerical results suggest the usefulness of this approach and show its potential for the application in optimization based navigation tasks. The proposed objectives, especially the minimum deviation objective, achieved the desired tasks and behaved qualitatively as expected. These objectives have conflicting aims in some situations, where they were penalized and degraded accordingly. The quaternion based state equations are given in the simple compact form of the first order ODEs and are useful for implementation in any numerical package. The tip orientation has so far been rarely considered in the literature, but appears to be useful for designing and planning more complex tasks. In the current study, only unloaded robots are considered. The given methodology can



be extended from zero load to loaded cases after using the state equations from the geometrically exact model (Rucker et al., 2010). The presented objectives may have less conflicting effect on each other when highly flexible CTCRs with more tubes are used. In such situations, they have multiple configurations for any required objective and the conflicting objectives could find a compromise solution satisfying the requirements. However, it is computationally complex to solve problems with more than three tubes. Obstacle avoidance can be considered by including the objective function (Lyons et al., 2009; Flaßkamp et al., 2019) to the presented framework.

## ACKNOWLEDGEMENTS

The research of Dhanakoti and Maddocks has been funded by the Einstein Foundation Berlin.

## REFERENCES

- Alfalahi, H., Renda, F., and Stefanini, C. (2020). Concentric tube robots for minimally invasive surgery: Current applications and future opportunities. *IEEE Trans. Med. Robot. Bion.*
- Baykal, C., Torres, L. G., and Alterovitz, R. (2015). Optimizing design parameters for sets of concentric tube robots using sampling-based motion planning. In *2015 IEEE/RSJ International Conference on Intelligent Robots and Systems (IROS)*, pages 4381–4387.
- Bergeles, C., Gosline, A. H. C., Vasilyev, N. V., Codd, P. J., del Nido, P. J., and Dupont, P. E. (2015). Concentric tube robot design and optimization based on task and anatomical constraints. *IEEE Transactions on Robotics*, 31:67–84.
- Betts, J. T. (2010). *Practical Methods for Optimal Control and Estimation Using Nonlinear Programming, Second Edition*. Society for Industrial and Applied Mathematics, second edition.
- Burgner, J., Rucker, D. C., Gilbert, H. B., Swaney, P. J., Russell, P. T., Weaver, K. D., and Webster, R. J. (2013). A telerobotic system for transnasal surgery. *IEEE/ASME transactions on mechatronics : a joint publication of the IEEE Industrial Electronics Society and the ASME Dynamic Systems and Control Division*, 19(3):996–1006.
- Burgner, J., Swaney, P. J., Rucker, D. C., Gilbert, H. B., Nill, S. T., Russell, P. T., Weaver, K. D., and Webster III, R. J. (2011). A bimanual teleoperated system for endonasal skull base surgery. In *2011 IEEE/RSJ International Conference on Intelligent Robots and Systems*, pages 2517–2523.
- Dichmann, D. J., Li, Y., and Maddocks, J. H. (1996). Hamiltonian formulations and symmetries in rod mechanics. In Mesirov, J. P., Schulten, K., and Summers, D. W., editors, *Mathematical approaches to biomolecular structure and dynamics*, pages 71–113. Springer.
- Flaßkamp, K., Worthmann, K., Mühlhoff, J., Greiner-Petter, C., Büskens, C., Oertel, J., Keiner, D., and Sattel, T. (2019). Towards optimal control of concentric tube robots in stereotactic neurosurgery. *Mathematical and Computer Modelling of Dynamical Systems*, 25(6):560–574.
- Garriga-Casanovas, A. and y Baena, F. R. (2018). Complete follow-the-leader kinematics using concentric tube robots. *The International Journal of Robotics Research*, 37(1):197–222.
- Gilbert, H. B., Hendrick, R. J., and Webster, R. J. (2016). Elastic stability of concentric tube robots: A stability measure and design test. *IEEE transactions on robotics : a publication of the IEEE Robotics and Automation Society*, 32(1):20–35.
- Gilbert, H. B., Neimat, J., and Webster, R. J. (2015). Concentric tube robots as steerable needles: Achieving follow-the-leader deployment. *IEEE Transactions on Robotics*, 31(2):246–258.
- Granna, J., Godage, I. S., Wirz, R., Weaver, K. D., Webster, R. J., and Burgner-Kahrs, J. (2016). A 3-d volume coverage path planning algorithm with application to intracerebral hemorrhage evacuation. *IEEE Robotics and Automation Letters*, 1(2):876–883.
- Griewank, A. and Walther, A. (2000). Evaluating derivatives - principles and techniques of algorithmic differentiation, second edition. In *Frontiers in applied mathematics*.
- Kierzenka, J. A. and Shampine, L. F. (2008). A BVP solver that controls residual and error. *JNAIAM J. Numer. Anal. Ind. Appl. Math.*, pages 1–2.
- Lyons, L. A., Webster, R. J., and Alterovitz, R. (2009). Motion planning for active cannulas. In *2009 IEEE/RSJ International Conference on Intelligent Robots and Systems*, pages 801–806.
- Nocedal, J. and Wright, S. (2006). *Numerical Optimization*. Springer.
- Rucker, D. C., Jones, B. A., and Webster III, R. J. (2010). A geometrically exact model for externally loaded concentric-tube continuum robots. *IEEE transactions on robotics : a publication of the IEEE Robotics and Automation Society*, 26(5):769–780.
- Rucker, D. C. and Webster, R. J. (2011). Computing Jacobians and compliance matrices for externally loaded continuum robots. In *2011 IEEE International Conference on Robotics and Automation*, pages 945–950.
- Rucker, D. C., Webster III, R. J., Chirikjian, G. S., and Cowan, N. J. (2010). Equilibrium conformations of concentric-tube continuum robots. *The International Journal of Robotics Research*, 29(10):1263–1280.
- Yip, M. C., Sganga, J., and Camarillo, D. B. (2017). Autonomous control of continuum robot manipulators for complex cardiac ablation tasks. *J. Medical Robotics Res.*, 2:1750002:1–1750002:13.